Spatiotemporal high-resolution mapping of biological production in the Southern Ocean

Supplementary Notes

1: Data standardization

In this study, we applied our hybrid DIC parameterization to T, S, DO, and Pr from 2004 to 2019 measured in 27,039 cycles of 154 BGC-Argos and obtained DIC spatiotemporal distribution over the SO. To obtain the NCP in the water column, we integrated the amount of DIC variation in the production period within the water column as the NCP, which was obtained by subtracting the predicted DIC (DIC_{pre}) at the beginning of the production period from the DIC_{pre} at the end of that production period at the same depth. For RES, the operation is the same as for NCP, but for the Restoration period (see Method section "**Estimation of NCP and RES**" for details). However, because the BGC-Argo depth data varied from one measurement cycle to another, the depth of each DIC_{pre} for each measurement cycle we predicted was different. Therefore, it was essential to standardize the depth of each DIC_{pre} in the SO water column at the following standard depth levels: 5, 10, 20, 30, 40, 50, 60, 70, 80, 90, 100, 125, 150, 175, and 200 m. Because biological productivity is limited to the euphotic zone, we assumed a maximum depth of 200 m for the DIC_{pre} determined in this study. We then conducted DIC_{pre} depth standardization by linearly interpolating the observed depth-layer data to the standard depth level.

2: Introduction of DIC Parameterization methods

2.1: Multiple Linear Regression (MLR)

MLR is a simple and well-known technique for establishing a linear relationship between the independent and dependent variables. It can also be used to judge the validity of each input parameter. We used hydrographic data for T, S, DO, and Pr as parameters for DIC parameterization in the SO (Fig. S2a, see Table S3 for the details of the validity of each parameter).

The DIC_{pre} expression derived from the MLR is：

$$DIC_{pre} = 983.2 - 8.557 \cdot T + 34.6 \cdot S + 0.5766 \cdot AOU + 1.787\times10^{-3} \cdot Pr, \quad \text{(S1)}$$

(number of data points (n) = 48,812; coefficient of determination (R^2) = 0.99;

Root mean square error (RMSE) = 6.1 μmol kg^{-1})

where AOU is the apparent oxygen utilization computed from the DO and saturated DO concentration. Details of the data constraints of the MLR method used in this study are listed in Table S2.

Although MLR can elucidate the correlation between the independent and dependent variables, when it is applied to DIC reconstruction in the surface mixed layer of SO, the independent variable is influenced by factors external to the ocean in the dependent variable due to the complex biological and physical processes in the surface mixed layer. This results in a non-linear relationship such that MLR is not applicable to the surface mixed layer of SO (Fig. S2e, Table S2).

2.2: Neural Network (NN)

We used neural network technology with a back-propagation function. The network comprised an input, hidden, and output layer. The number of nodes in the input layer corresponds to the number of variables describing the test attribute. Conversely, the number of neurons in the output layer is equal to the number of classes. The number of hidden layers and neurons depends on the complexity of the task and the amount of training data. In both the hidden and output layers, each neuron is connected to all nodes of the subsequent layers by an associated numerical weight. The weights that connect the two neurons control the size of the signal between them. A supervised training approach was utilized to train the neural network (n = 56,412; Fig. S2b), the level of which was controlled by the validation error in the subsequent testing phase (n = 14,103; Fig. S2c).

DIC_{pre} expression derived from the NN is：

$$DIC_{pre} = 2208 - 49.73 \cdot \mathrm{TanH}\,(0.5 \cdot (5.326 + 0.2797 \cdot T - 0.2376 \cdot S - 0.008928 \cdot AOU - 0.0002357 \cdot Pr)) + 74.51 \cdot \mathrm{TanH}\,(0.5 \cdot (-46.90 - 0.1520 \cdot T + 1.369 \cdot S + 0.01135 \cdot AOU - 0.0005855 \cdot Pr)) + 75.15 \cdot \mathrm{TanH}\,(0.5 \cdot (14.52 - 0.1890 \cdot T - 0.5602 \cdot S + 0.02151 \cdot AOU + 0.0006968 \cdot Pr)), \quad \text{(S2)}$$

(number of data points (n) = 70,515; coefficient of determination (R^2) = 0.98.

Root mean square error (RMSE) = 7.5 μmol kg^{-1})

where TanH means hyperbolic tangent function, and the TanH in the neural network is a function that converts any input value into a number in the range of –1.0 to 1.0 and outputs it.

A comparison of observed and predicted DIC concentrations in the SO demonstrates that NN can more accurately and effectively reconstruct DIC over the SO, including the surface mixed layer, than MLR (Figs. S2d, S2e, and S2f).

3: Gridding of NCP and RES data

We estimated our NCP and RES in the entire SO by using the weighted average algorithm as a common gridding method utilizing the Ocean Data View (ODV) software (see Ocean Data View User's Guide version 5.1.0, 16.6.1)[3]. To achieve this, we first constructed a grid on the SO, and the grid resolution can be assigned as required. In this study, the two-dimensional (2D) grid horizontal resolution for the entire SO was 1° × 1°.

After constructing the grid for the SO, ODV allows us to compute the attribute estimates of the NCP for each grid point using a simple weighted averaging scheme (see Equation S3).

$$c_e = \sum_i \alpha_i \cdot d_i / \sum_i \alpha_i \qquad \text{(S3)}$$

The weight α_i of the data points decreases exponentially with increasing distance between the data and grid points: $\alpha_i = e^{-r}$, with $r = (\Delta x/L_x)^2 + (\Delta y/L_y)^2$, where Δx and Δy are the distances between the data and grid points in the X and Y directions, respectively, and L_x and L_y are independent average length scales in the X and Y directions, respectively. The length scales in the X- and Y-directions in the two-dimensional grid estimated by repeating the lines were 80 permille.

4: Uncertainties of NCP, RES and CS

The uncertainties in our estimation of NCP and RES were predominantly derived from two steps, “inventory” and “gridding” errors.

4.1: Inventory error

It is the uncertainty arising from the root mean square error (RMSE) in our parameterizations, which reflects DIC_{pre} accuracy. When vertically integrating NCP and/or RES for each depth level to estimate tNCP and/or tRES, the propagation of error from RMSE in this procedure leads to a final uncertainty as an "inventory error" of 6%.

4.2: Gridding error

It is the uncertainty derived from the gridding operation. According to Section **S3** (Gridding of NCP and RES data), we predicted the NCP and/or RES for regions where no BGC-Argo data were available. The uncertainty arising from this procedure is termed the "gridding error". To quantify this gridding error, we conducted the same gridding for BGC-Argo DO data and compared the gridded DO data with observation-based DO climatology data from the World Ocean Atlas 2018 (WOA18). We found that the gridding operation generated an average difference of approximately 7% in regions where no BGC-Argo data were available.

In the NCP and RES distributions (Fig. S4), we demonstrated only the data points of the location of BGC-Argo at the beginning of the Production and Restoration periods, as BGC-Argo is constantly moving with ocean currents. When computing the gridding error, we assumed the gridding error in the regions with BGC-Argo passing through as zero, and considered the gridding error in the regions with no BGC-Argo passing through as 7%, resulting in 3% of an area-weighted gridding error over the SO. Note that the error may be larger due to the lack of data for the Antarctic coast (Fig. S3).

4.3: Total error

Considering the combination of the inventory and the gridding error, we obtain the total uncertainties of NCP ($U_{\_NCP}$) and RES ($U_{\_RES}$) of 6.5% as the propagation of error, as follows:

$$U_{\_NCP} = U_{\_RES} = \sqrt{(\text{inventory error}^2 + \text{gridding error}^2)} \qquad \text{(S4)}$$

The total uncertainty of the Carbon Sink ($U_{\_CS}$) can be obtained using the following equation:

$$U_{\_CS} = \sqrt{(U_{\_NCP}{}^2 + U_{\_RES}{}^2)} \qquad \text{(S5)}$$

5: Uncertainties of time series of NCP and RES

The time series of NCP and RES (mol-C m^{-2} $year^{-1}$) over the mid-SO from 2008 to 2017 is calculated by averaging the tNCP and tRES with the grid number. The uncertainties are shown as one standard deviation. However, because of the spatial bias of data for each year, the uncertainties for each year may be larger than shown in Fig.3a.

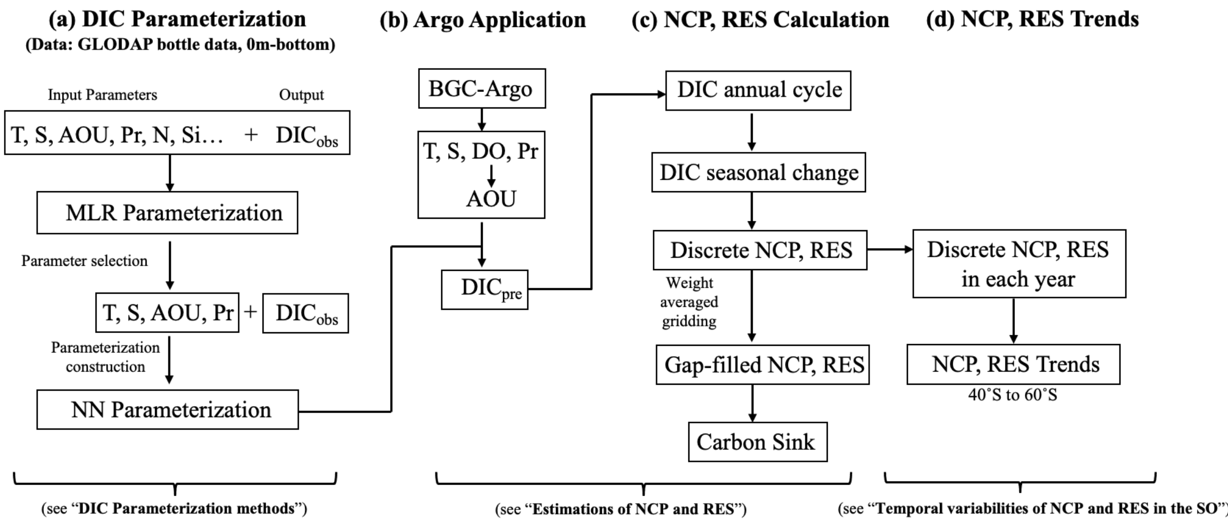

Fig. S1 The flow chart of the estimations in this study. (a) The construction of the DIC parameterization. Here, we used MLR for the parameter selection and used back-propagation NN for the parameterization construction. (b) Application of our DIC parameterization to the BGC-Argo dataset. (c) Using the predicted DIC dataset to estimate NCP and RES. (d) Estimation of trends of NCP and RES.

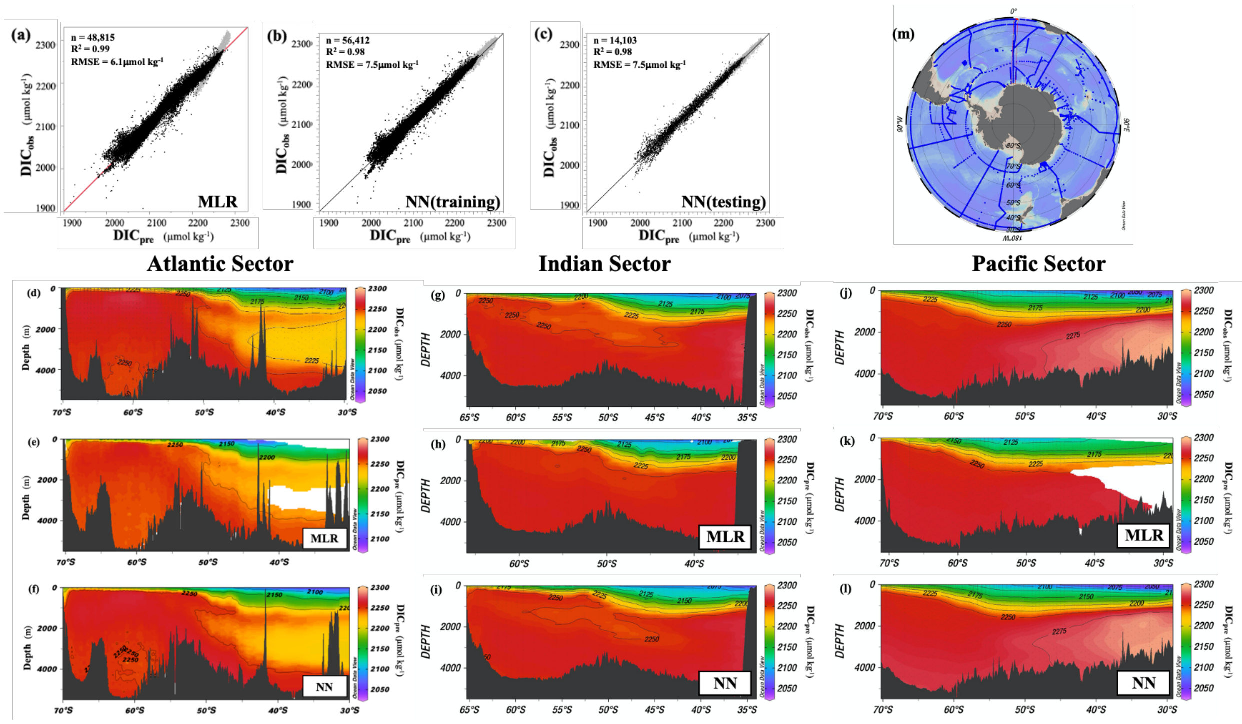

Fig. S2. Relationship between predicted (DIC_{pre}) (µmol kg^{-1}) and observed DIC (DIC_{obs}) (µmol kg^{-1}) from 0–6000 m in the SO. (a) DIC_{pre} of MLR versus DIC_{obs}. (b) DIC_{pre} of NN with training dataset versus DIC_{obs}, where "training dataset" means the dataset used to train NN for reconstructing DIC. (c) Same as (b), but DIC_{pre} of NN with testing, where "testing" means the dataset used to validate the result of NN training. Black dots show the data in the upper 200m. (d-l) The vertical section of DIC_{obs} and DIC_{pre} (µmol kg^{-1}) from 0–6000 m in the Atlantic sector (d-f), Indian sector (g-i) and Pacific sector (j-l) of SO. The white areas in this figure indicate the areas where DIC cannot be reconstructed due to the constraints of the MLR method. See Table S2 for the constraints. The notation "n" indicates the number of data points; R^2 indicates the coefficient of determination; RMSE indicates the root mean square error. (m) Observational data used for constructing DIC parameterizations.

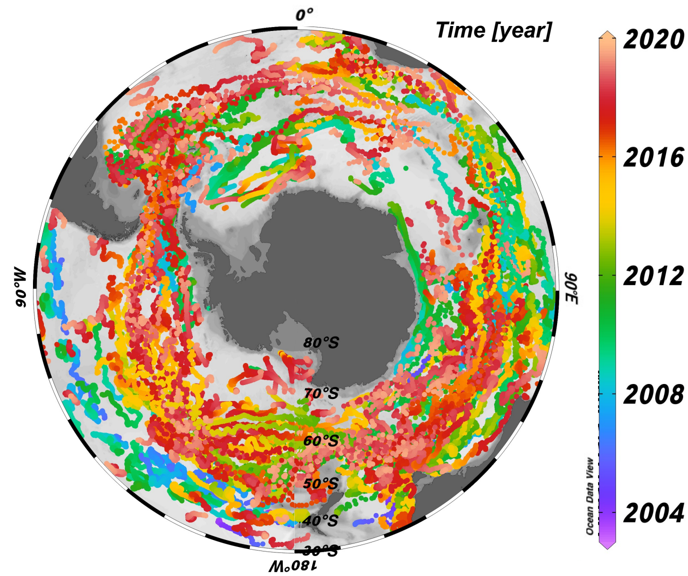

145 **Fig. S3. BGC-Argo trajectories in the SO with trajectories in different years are depicted by colored dots from 2004 to 2019.** The number of BGC-Argo is 154, with 27,039 vertical profiles. BGC-Argo: biogeochemical Argo float. This figure was drawn using Ocean Data View[1].

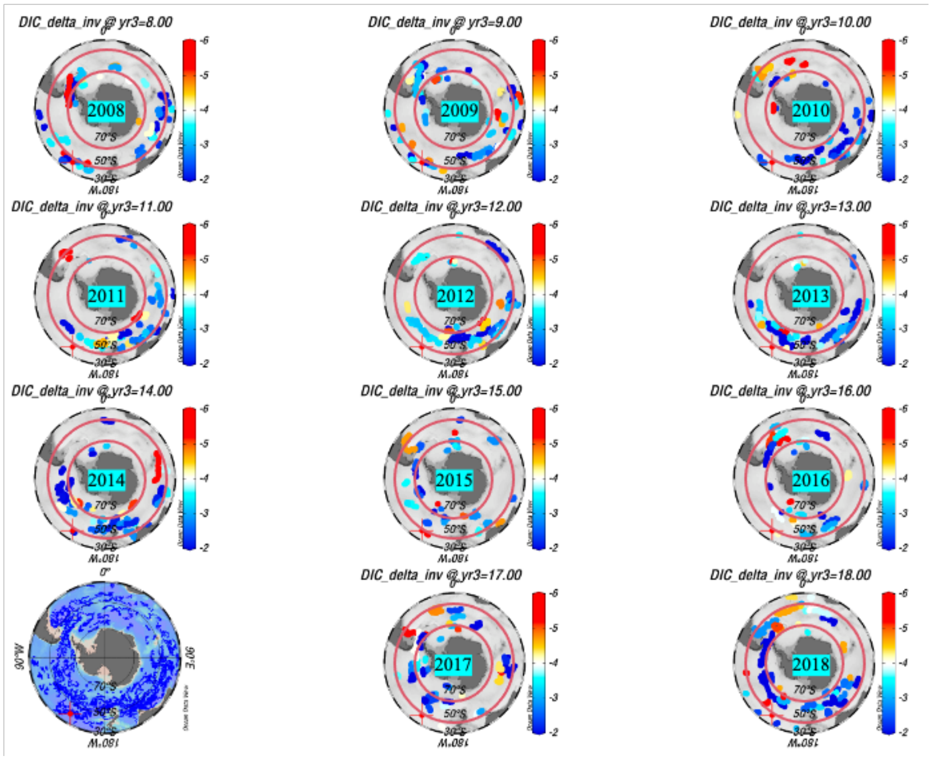

Fig. S4. Location and value of NCP data in the SO from 2008 to 2018 (mol-C m^{-2} year^{-1}). The number of all NCP estimated in this study is 484, and color dots indicate the observed BGC-Argo trajectories during the biological production period. Data distribution of each year. Because the data from 2008 to 2018 are distributed throughout the SO, and the BGC-Argo are mostly concentrated between the red circles (45˚S to 60˚S), we used the data between the red circles from 2008 to 2018 to obtain the NCP and RES time series over the SO (Fig. 3a). These figures are drawn using Ocean Data View[1].

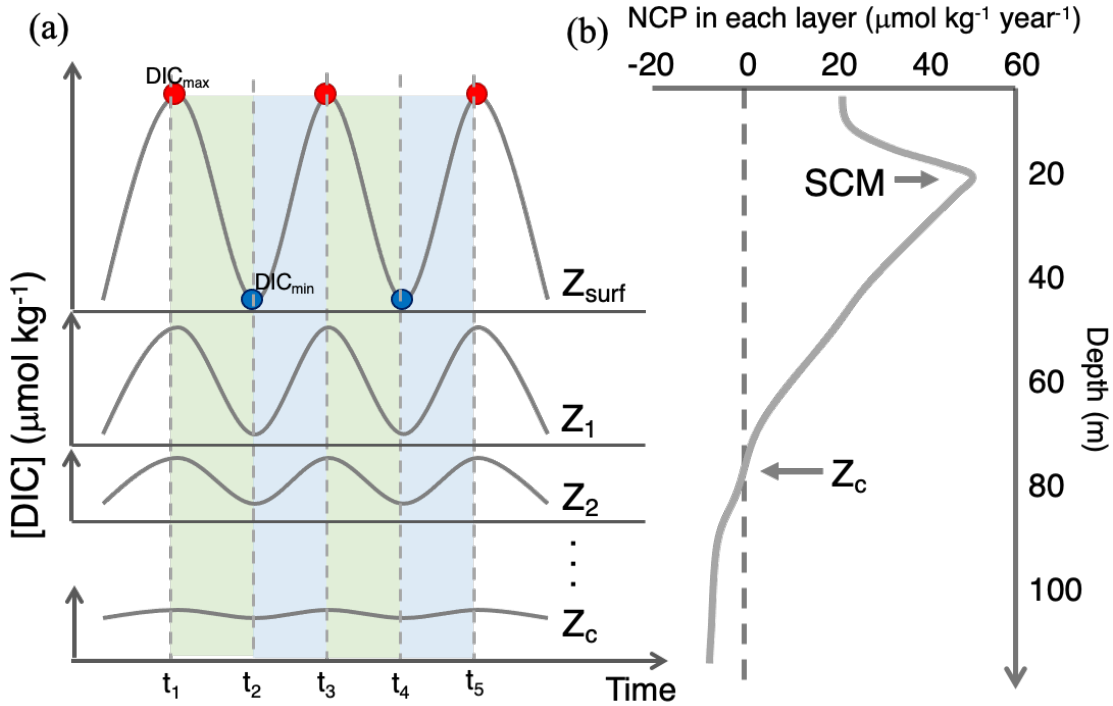

Fig. S5. Schematic figures for the definition of NCP and RES in this study. (a) Time series of DIC concentration (DIC) in each standard layer. Z_{surf} indicates the surface depth, Z_1, and Z_2 indicate the deeper standardized depth determined in Supplementary text A1, and Z_c indicates the critical depth. The maximum and minimal values of the DIC cyclical variation in each layer are referred to as DIC_{max} and DIC_{min}, depicted by red and blue points. NCP in each layer is defined as the decrease from DIC_{max} to DIC_{min}. (b) The vertical profiles of NCP in each layer. Z_c is defined as the depth where NCP becomes zero or the minimal value. The SCM is also marked in this figure.

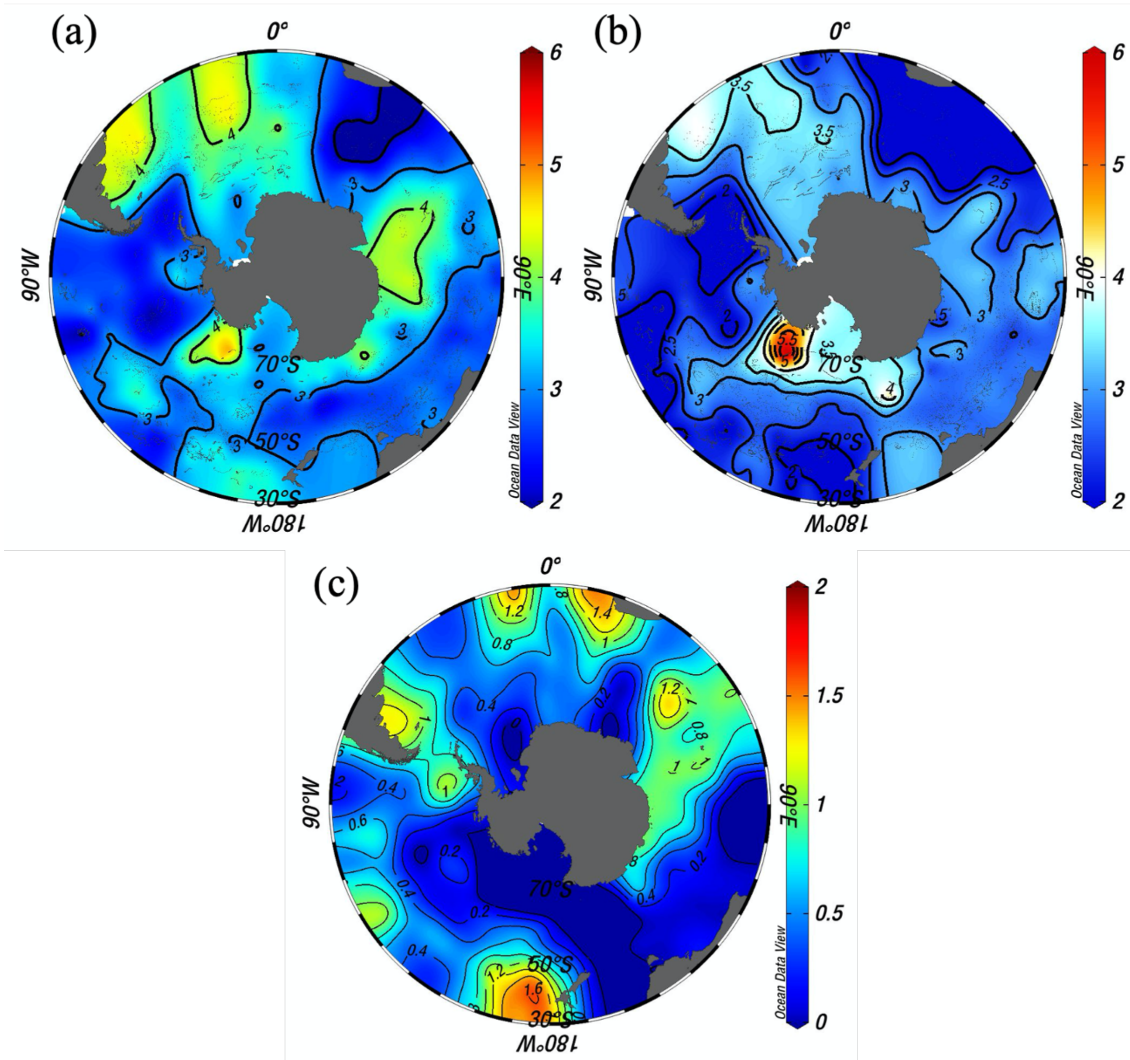

Fig. S6. Distribution of (a) NCP (mol-C m^{-2} year^{-1}), (b) RES (mol-C m^{-2} year^{-1}), and (c) CS (mol-C m^{-2} year^{-1}) based on 154 BGC-Argo data during 2004 – 2019. Black dots indicate the observed data points through the BGC-Argo trajectories during the biological production period. NCP and RES were extended to the entire SO (south of 30˚S) by using the weight average algorithm based on the NCP and RES observed data points. These figures were drawn using Ocean Data View[1].

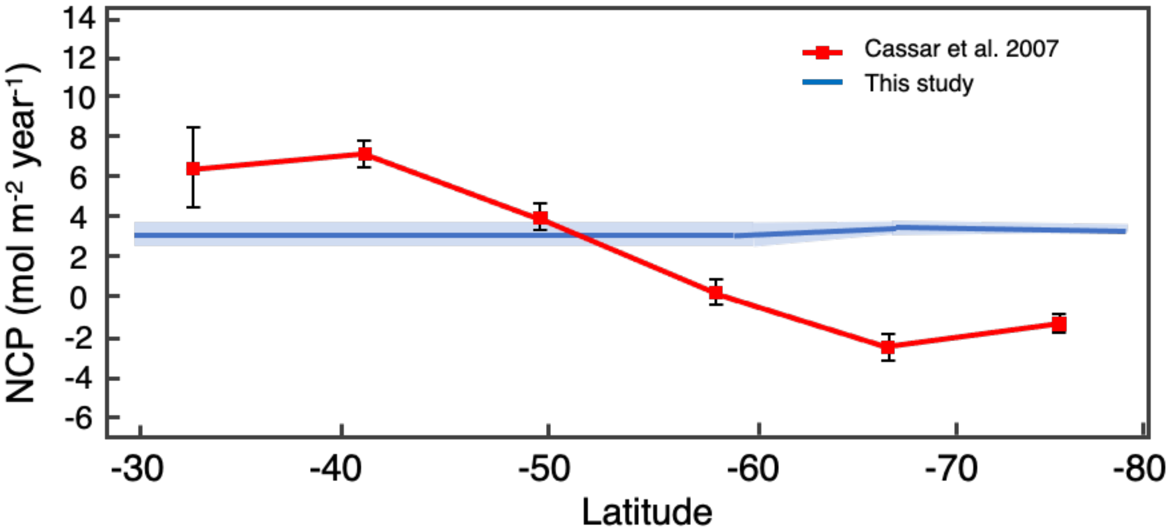

Fig. S7. Comparison of NCP in the SO between our result and the previous study. The red line indicates the meridional distribution of NCP estimated by Cassar et al. (2007)[2] using O_2/Ar within the surface mixed layer. This estimation was derived from averaging approximately one week of observations in each season, with the observations concentrated in the Indian sector. The blue line indicates the averaged meridional distribution of NCP estimated by this study upper the critical depth. The blue shad shows the standard deviation.

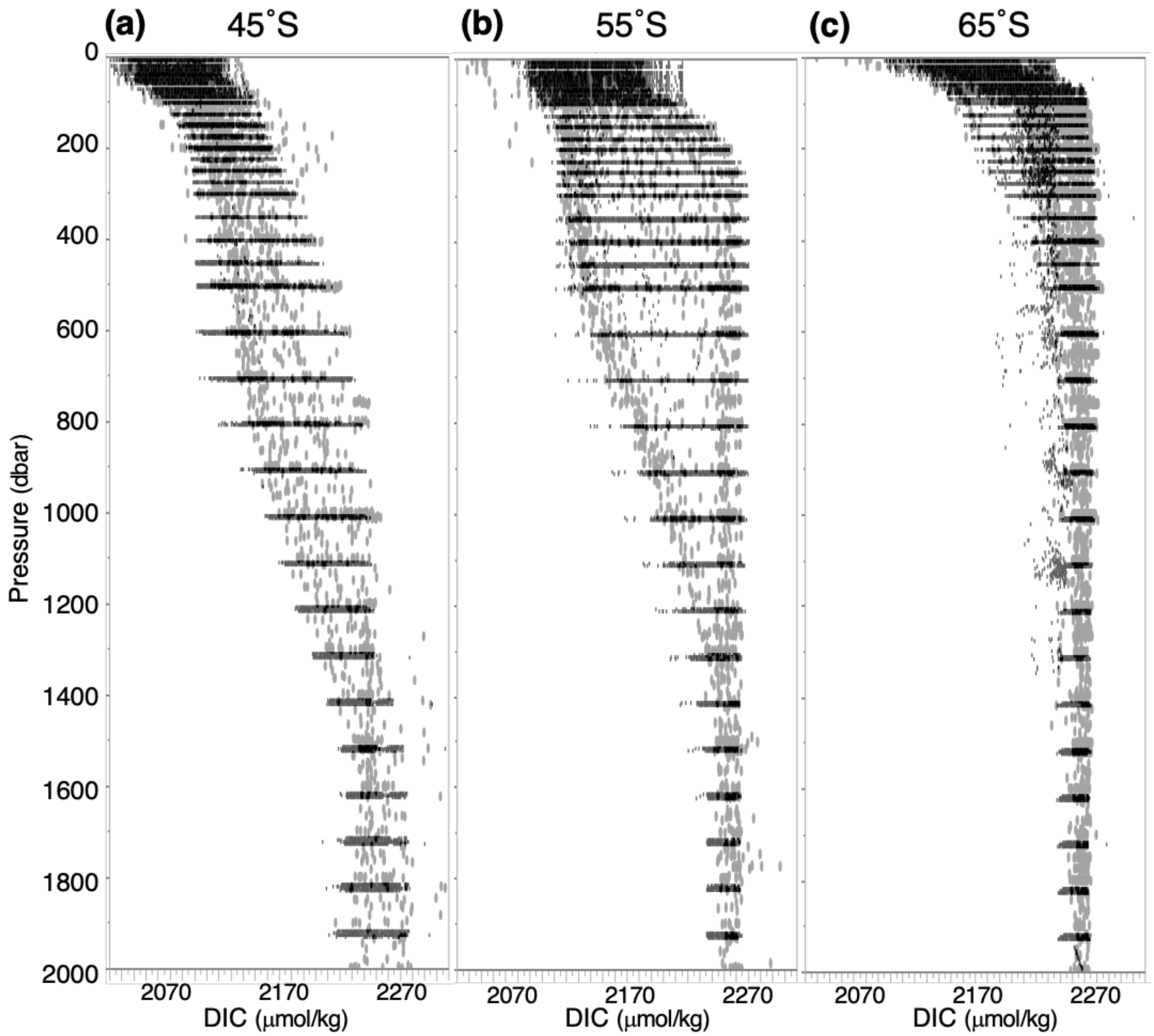

Fig. S8 Comparison plots of BGC Argo-derived DIC_{pre} and GLODAP DIC observations around Antarctica. (a) 45˚S, (b) 55˚S, (c) 65˚S. Black dots indicate the DIC_{pre} derived from BGC Argo data and gray dots indicate the GLODAP DIC observations.

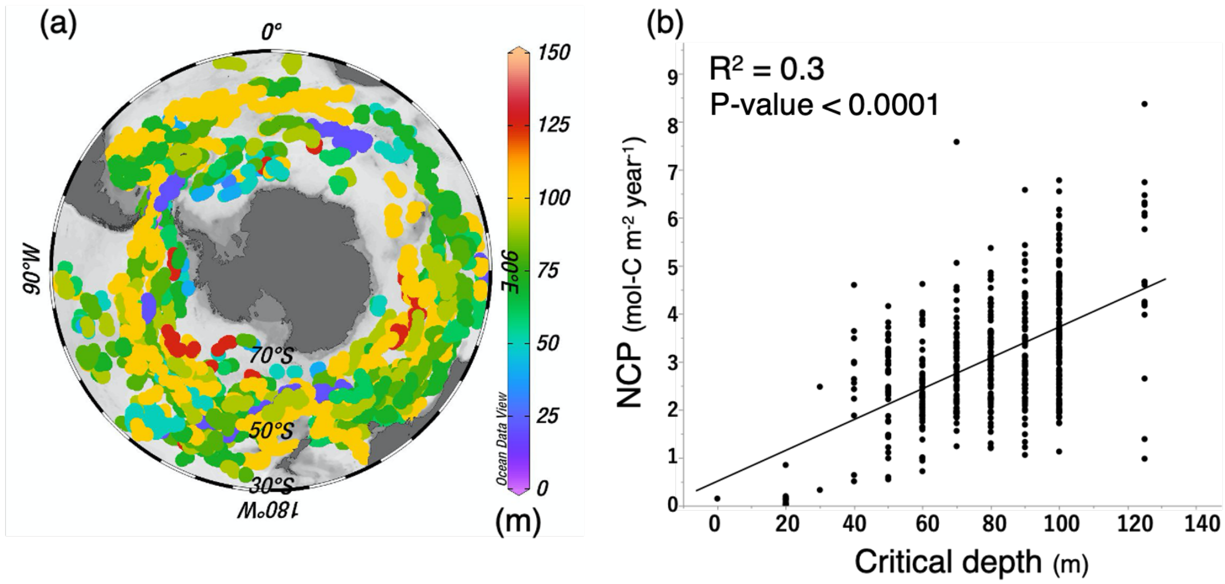

Fig. S9 Critical depth in the SO. (a) Mapping of the critical depth in the SO. The critical depth in this study is defined as the depth where the NCP becomes zero (see Fig. S5). (b) The correlation between the critical depth and the NCP in this study, with a determination coefficient (R^2) of 0.3.

Table S1

Information of BGC-Argo dataset undertaken for estimating the DIC concentrations from JAMSTEC (http://www.jamstec.go.jp/ARGO/argo_web/argo/) **in this study.** Latitude and longitude represent the position where the BGC-Argo started measuring after being deployed into the ocean. A negative latitude means south of the Equator, and a negative longitude means west of the Prime Meridian. WMO# is the World Meteorological Organization designation for the BGC-Argo. The BGC-Argo trajectories are shown in Fig. S3. We display the date of BGC-Argo as year-month-day.

NO.	WMO#	longitude	latitude	Date (Start)	Date (End)
1	1900722	76.753	-38.229	2007-02-21	2009-09-03
2	1901134	74.746	-38.903	2009-03-05	2014-10-05
3	1901135	90.828	-57.635	2009-08-24	2012-08-08
4	1901155	60.119	-46.340	2011-08-21	2018-08-14
5	1901157	95.120	-54.560	2011-10-21	2018-09-14
6	1901159	87.186	-47.192	2011-09-22	2015-08-12
7	1901207	17.345	-39.342	2011-03-01	2015-03-30
8	3900333	-111.328	-38.135	2006-03-15	2010-02-24
9	3900334	-99.401	-38.727	2006-03-02	2010-08-30
10	3900344	-115.121	-38.588	2006-03-15	2008-02-22
11	3900345	-106.432	-40.694	2006-02-07	2007-09-16
12	3900346	-95.687	-38.468	2006-02-25	2009-09-12
13	3901466	-98.931	-45.632	2013-02-15	2013-09-01
14	4900474	93.484	-51.603	2007-07-09	2010-02-09
15	4900475	103.092	-46.245	2007-09-12	2013-02-05
16	4900476	100.842	-48.101	2007-08-31	2011-09-03
17	4900483	98.722	-39.591	2007-09-06	2011-08-30
18	4900485	94.402	-33.220	2007-08-30	2011-09-02
19	5900421	-171.196	-41.163	2004-03-01	2004-09-07
20	5900841	141.114	-49.013	2005-08-14	2012-02-18
21	5900965	-172.326	-44.135	2006-02-16	2010-02-12
22	5900966	-174.137	-44.818	2006-02-03	2009-08-05
23	5901043	-160.164	-42.760	2006-03-15	2009-08-22

Table S1: (Continued)

NO.	WMO#	longitude	latitude	Date (Start)	Date (End)
24	5901044	-160.942	-42.498	2006-03-08	2009-08-07
25	5901045	-161.376	-43.381	2006-02-18	2010-02-22
26	5901046	-158.978	-47.680	2006-02-19	2010-02-07
27	5901047	-153.709	-46.380	2006-02-13	2009-08-16
28	5901048	-143.233	-44.648	2006-03-10	2009-09-01
29	5901050	-141.572	-43.644	2006-02-23	2010-02-19
30	5901051	-146.872	-43.008	2006-03-16	2010-09-13
31	5901052	-139.056	-41.177	2006-03-10	2010-08-30
32	5901054	-122.544	-40.053	2006-02-25	2010-02-14
33	5901187	153.018	-48.229	2007-08-26	2013-02-15
34	5901444	-84.078	-64.954	2008-02-05	2010-08-12
35	5901446	-87.435	-67.802	2008-03-11	2010-10-30
36	5901447	-73.506	-62.124	2008-03-11	2010-07-07
37	5901448	-50.670	-58.675	2008-03-31	2010-08-25
38	5901450	-66.209	-63.586	2008-02-20	2009-07-21
39	5901492	33.448	-49.718	2008-03-14	2010-03-17
40	5901644	140.240	-43.906	2008-09-23	2012-09-12
41	5901646	88.500	-42.486	2008-09-05	2014-03-08
42	5901647	106.929	-51.872	2008-09-29	2016-03-01
43	5901696	109.804	-38.095	2009-08-30	2011-03-13
44	5901697	111.991	-40.625	2009-08-21	2014-09-04
45	5901699	119.098	-56.561	2009-10-02	2016-08-06
46	5901730	8.479	-55.966	2008-09-24	2009-09-12
47	5901731	-7.645	-64.473	2008-10-17	2009-10-10
48	5901736	7.479	-57.102	2008-09-17	2008-09-17
49	5901739	-39.827	-65.032	2008-10-03	2011-02-13
50	5901744	-38.163	-65.792	2008-09-19	2011-10-08
51	5902101	98.184	-52.246	2009-09-15	2009-09-15
52	5902112	-69.026	-58.713	2009-09-29	2011-09-02
53	5902116	-114.492	-66.584	2009-09-10	2012-07-27

Table S1: (Continued)

NO.	WMO#	longitude	latitude	Date (Start)	Date (End)
54	5903218	141.640	-45.564	2009-09-05	2013-09-04
55	5903226	142.411	-45.284	2010-03-14	2014-09-24
56	5903242	142.934	-47.659	2010-09-14	2014-09-30
57	5903248	155.475	-58.423	2010-09-01	2018-08-30
58	5903256	151.348	-55.503	2010-08-21	2015-08-07
59	5903258	148.058	-47.540	2010-08-21	2016-02-29
60	5903259	143.977	-42.425	2010-09-11	2014-09-10
61	5903260	162.943	-58.681	2010-10-10	2018-09-08
62	5903614	-1.988	-64.372	2012-09-30	2014-10-20
63	5903615	0.692	-66.813	2012-02-28	2015-09-24
64	5903719	176.150	-59.813	2012-08-05	2014-09-04
65	5903721	-171.259	-64.493	2012-10-15	2014-06-25
66	5903939	160.805	-55.864	2012-07-12	2016-10-08
67	5904104	153.380	-64.202	2013-10-12	2017-02-11
68	5904179	-175.160	-58.744	2014-08-29	2018-10-03
69	5904180	-157.316	-66.062	2014-10-02	2018-09-13
70	5904184	-148.335	-63.300	2014-09-04	2017-10-03
71	5904185	-121.879	-60.076	2015-03-14	2018-02-20
72	5904223	-159.640	-43.382	2013-03-29	2013-09-10
73	5904395	-149.075	-39.085	2014-09-17	2017-03-06
74	5904396	-139.003	-54.524	2014-07-22	2015-07-29
75	5904397	-1.301	-61.810	2015-09-26	2018-09-22
76	5904467	4.103	-60.558	2015-09-18	2018-02-28
77	5904468	2.178	-64.668	2015-09-23	2016-09-28
78	5904469	0.636	-53.834	2015-04-04	2018-01-29
79	5904470	143.096	-47.347	2015-08-08	2016-09-24
80	5904471	1.747	-66.161	2015-09-14	2018-09-22
81	5904472	-11.908	-68.344	2015-09-22	2018-02-24
82	5904473	41.443	-48.601	2015-09-12	2015-09-12
83	5904658	-47.388	-53.088	2016-08-03	2018-09-08

Table S1: (Continued)

NO.	WMO#	longitude	latitude	Date	Date

				(Start)	(End)
84	5904659	-35.870	-57.040	2016-08-22	2018-07-28
85	5904672	-159.281	-60.831	2017-02-22	2017-09-01
86	5904673	-167.632	-60.139	2016-08-21	2017-02-07
87	5904678	145.224	-47.612	2016-08-13	2018-08-17
88	5904679	82.362	-55.730	2016-09-13	2018-08-31
89	5904694	-167.789	-34.543	2017-02-25	2018-08-27
90	5904695	-157.508	-55.421	2017-02-17	2018-09-19
91	5904761	-157.750	-47.715	2017-02-09	2018-08-09
92	5904766	-165.994	-57.600	2016-09-23	2018-10-24
93	5904767	-150.848	-58.981	2017-03-01	2018-08-25
94	5904841	-103.620	-43.401	2017-08-12	2018-08-29
95	5904845	-83.061	-61.220	2017-08-30	2018-09-05
96	5904854	-52.725	-50.486	2017-06-06	2018-08-13
97	5904855	-85.129	-68.013	2017-09-22	2017-09-22
98	5904856	-58.411	-59.286	2017-08-19	2018-08-17
99	5904859	-102.934	-69.995	2017-10-13	2018-03-23
100	5904980	-65.265	-62.383	2017-08-22	2018-08-02
101	5904982	-52.081	-51.536	2017-07-08	2017-07-08
102	5904984	-46.033	-58.968	2017-10-06	2018-08-22
103	5905069	106.489	-53.470	2017-08-22	2018-09-19
104	5905070	97.671	-53.364	2017-09-01	2018-10-21
105	5905072	71.491	-45.187	2017-04-06	2018-09-11
106	5905073	68.673	-46.155	2017-04-06	2018-09-30
107	5905075	-105.785	-67.948	2017-10-04	2018-02-22
108	5905076	-111.214	-53.318	2017-09-01	2018-08-30
109	5905077	-110.015	-65.578	2017-09-17	2017-09-17
110	5905079	-111.725	-55.240	2017-08-14	2018-09-12
111	5905099	-176.462	-61.091	2017-09-14	2018-08-22
112	5905100	167.888	-65.474	2017-09-26	2018-02-24
113	5905103	131.852	-57.020	2018-07-26	2018-07-26

Table S1: (Continued)

NO.	WMO#	longitude	latitude	Date	Date

NO.	WMO#	longitude	latitude	Date (Start)	Date (End)
114	5905104	-134.347	-31.774	2018-03-30	2018-09-26
115	5905107	-154.533	-33.493	2018-03-09	2018-09-16
116	5905109	-114.322	-33.523	2018-03-20	2018-09-16
117	5905131	10.036	-32.207	2018-03-09	2018-09-05
118	5905132	-8.637	-34.665	2018-03-06	2018-09-03
119	5905134	-5.412	-44.412	2018-03-19	2018-09-16
120	5905135	-8.644	-46.571	2018-03-01	2018-09-18
121	5905368	63.173	-56.999	2018-08-31	2018-08-31
122	5905371	141.922	-54.486	2018-08-23	2018-08-23
123	5905372	139.189	-56.775	2018-07-26	2018-07-26
124	5905375	140.004	-63.210	2018-07-21	2018-07-21
125	5905376	168.413	-57.162	2018-08-01	2018-08-01
126	6900896	19.584	-36.832	2011-01-17	2014-12-27
127	6900954	4.109	-41.264	2012-08-30	2016-03-02
128	6903233	157.704	-54.030	2018-09-04	2018-09-04
129	1901154	79.290	-48.628	2011-09-29	2018-08-23
130	2900120	113.526	-63.933	2008-03-15	2010-02-14
131	5901445	38.322	-60.222	2008-10-17	2011-02-19
132	5901449	-91.041	-63.863	2008-02-19	2010-08-19
133	5901645	75.741	-38.613	2008-08-06	2015-09-09
134	5901648	89.799	-47.035	2008-08-25	2015-09-28
135	5901740	-41.029	-64.527	2008-09-19	2011-01-30
136	5901742	-40.566	-64.639	2008-09-20	2011-02-07
137	5902109	-96.544	-69.077	2009-10-19	2011-02-22
138	5902110	-75.422	-65.645	2009-08-31	2012-01-31
139	5903255	134.000	-50.222	2010-08-20	2014-08-29
140	5903593	96.057	-42.116	2012-09-12	2015-02-08
141	5903613	-2.754	-64.787	2012-02-26	2015-03-03
142	5903616	0.256	-65.599	2012-03-05	2015-09-23
143	5903649	143.981	-45.044	2011-09-03	2011-09-03

Table S1: (Continued)

NO.	WMO#	longitude	latitude	Date (Start)	Date (End)

144	5903678	146.820	-46.586	2011-09-12	2012-04-17
145	5903679	144.361	-45.599	2012-02-26	2013-02-11
146	5903717	177.443	-66.320	2012-10-29	2013-02-15
147	5903718	-162.813	-50.918	2012-08-02	2014-09-16
148	5903722	-175.085	-62.931	2012-10-07	2014-08-13
149	5904183	-148.561	-66.745	2014-10-03	2018-03-10
150	5904220	-173.520	-45.443	2013-03-20	2013-08-29
151	5904675	95.051	-41.113	2016-08-27	2018-09-21
152	5904860	-157.266	-72.528	2017-10-09	2018-03-29
153	5905023	99.451	-40.094	2016-03-10	2016-10-07
154	6903183	172.027	-48.795	2016-05-04	2017-11-10

Table S2

Constraint conditions for MLR parameterization of DIC in the SO.

Constraints		Remarks
Bottom depth	> 1500 m	Removing continental shelf
Mixed layer depth	ΔT > 0.5 °C [a]	ΔT ≤ 0.5 °C was not used
Salinity	34 – 35	
Water masses	Except NADW [b], SASW [c]	NADW: 34.8 < S < 35& 1.5 °C < T < 4 °C SASW: T > 8 °C[3]

[a] Mixed layer depth is defined as the depth at which temperature (T) changes by a given threshold value (ΔT; here, ΔT = 0.5 °C) relative to the temperature at the surface[4].

[b] North Atlantic Deep Water

[c] Subantarctic Surface Water

Table S3. Summary of MLR parameterization of DIC in this study.

Region	**Parameter**	***F*** [a]	***B*** [b]	**Standardized *β*** [c]	**VIF** [d]
SO	Intercept	–	983.2	–	–
	AOU	421,148	0.5765	0.54	1.92
	T	582,285	– 8.557	– 0.52	1.32
	S	33,629	34.60	0.15	1.95
	Pr	5,121	1.687×10^{-3}	0.05	1.46

[a] *F*-value with a significance level of $\alpha = 0.05$; significant when *F*-value over 2.4.
[b] Regression coefficient
[c] Standardized regression coefficient
[d] Variance Inflation Factor; indicates no multicollinearity when VIF is below 10

Supplementary References

1 Schlitzer, R. *Ocean Data View*, https://odv.awi.de (2020).

2 Cassar, N. *et al.* The Southern Ocean biological response to aeolian iron deposition. *Science* **317**, 1067-1070, doi:10.1126/science.1144602 (2007).

3 Emery, W. J. Water Types and Water Masses. in Ocean circulation. *Water Types and Water Masses*, 1556–1567 (2003).

4 de Boyer Montégut, C. Mixed layer depth over the global ocean: An examination of profile data and a profile-based climatology. *J. Geophys. Res.* **109**, doi:10.1029/2004jc002378 (2004).